Int. J. Nanoelectronics and Materials **3** (2010) 17-34

The dependence of saturation velocity on temperature, inversion charge and electric field in a nanoscale MOSFET

Ismail Saad[1,2,*] , Michael L. P. Tan[2], Mohammed Taghi Ahmadi[2], Razali Ismail[2], Vijay K. Arora[2,3]

[1]School of Engineering & IT, Universiti Malaysia Sabah, 88999, Sabah
[2]Faculty of Electrical Engineering, Universiti Technologi Malaysia, 81310, Johor
[3]Department of Electrical and Computer Eng., Wilkes University, PA 18766, USA

Abstract

The intrinsic velocity is shown to be the ultimate limit to the saturation velocity in a very high electric field. The unidirectional intrinsic velocity arises from the fact that randomly oriented velocity vectors in zero electric field are streamlined and become unidirectional giving the ultimate drift velocity that is limited by the collision-free (ballistic) intrinsic velocity. In the nondegenerate regime, the intrinsic velocity is the thermal velocity that is a function of temperature and does not sensitively depend on the carrier concentration. In the degenerate regime, the intrinsic velocity is the Fermi velocity that is a function of carrier concentration and independent of temperature. The presence of a quantum emission lowers the saturation velocity. The drain carrier velocity is revealed to be smaller than the saturation velocity due to the presence of the finite electric field at the drain of a MOSFET. The popular channel pinchoff assumption is revealed not to be valid for either a long or short channel. Channel conduction beyond pinchoff enhances due to increase in the drain velocity as a result of enhanced drain electric field as drain voltage is increased, giving a realistic description of the channel length modulation without using any artificial parameters. The velocity so obtained is considered in modeling the current-voltage characteristics of a MOSFET channel in the inversion regime and excellent agreement is obtained with experimental results on an 80-nm channel.

Keywords: Nano-MOSFET, Saturation Velocity, Quantum Confinement, Ballistic Carriers, High-Field Transport.
PACS: 85.35.-p,43.58.-e,85.35.Ds, 05.60.-k.

1. Introduction

The Metal-Oxide-Semiconductor Field Effect Transistor (MOSFET) of Fig. 1 is a vehicle for design of integrated circuits both for digital and analog applications. It has a long history of channel length being scaled down that now is in the nanometer regime. A large number of variations of the MOSFET have been tried to enhance performance, the most prominent being that of reducing the channel length in the nanometer regime. In spite of vast literature on MOSFET scaling, design, and VLSI applications, the fundamental

[*]) For Correspondence; Email: ismailsaad07@gmail.com.

processes [1] that control the performance of the channel in the MOSFET continue to elude physicists and engineers alike. There is ongoing debate over the interdependence of mobility that is controlled by momentum-randomizing scattering events and saturation velocity that depends on the streamlined motion of electrons. Most investigators tend to converge on the theme that the saturation velocity does not sensitively depend on the low-field mobility. However, there does not appear to be a consensus on the factors limiting the current and velocity. In a paradigm based on the distribution function developed by Arora [2], it is shown in [1] that the applied electric field streamlines velocity vectors giving saturation velocity that is limited by intrinsic velocity of carriers subject to further degradation by the onset of a quantum emission.

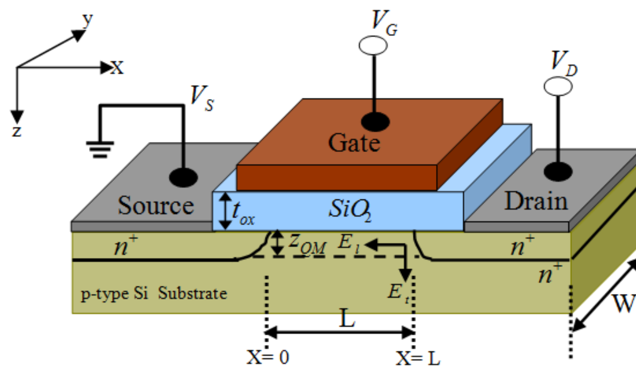

Fig. 1: Basic structure of an n-channel MOSFET with electrons removed from the Si/SiO_2 interface due to the quantum-confinement effect.

Fig. 1 demonstrates that in a nanoscale channel, where oxide thickness is a few nm, the separation of electrons from the interface due to the quantum-confinement effect cannot be ignored. The gate electric field Et does not heat electrons as it is not an accelerating field rather it is confining electric field that makes an electron a quantum entity described by wave character with discrete (digital) energy levels. The wavefunction vanishes at the Si/SiO2 interface and peaks at a distance approximately zQM away from the interface. This alters the gate capacitance and hence the carrier density in the channel. The mobility degradation due to this quantum confinement effect is described in Sec. II. Sec. III describes the charge transport driven by the longitudinal electric field that is distinctly high in nanoscale channels. This channel electric field degrades the mobility resulting in velocity saturation. The ultimate saturation velocity is ballistic as will be shown.

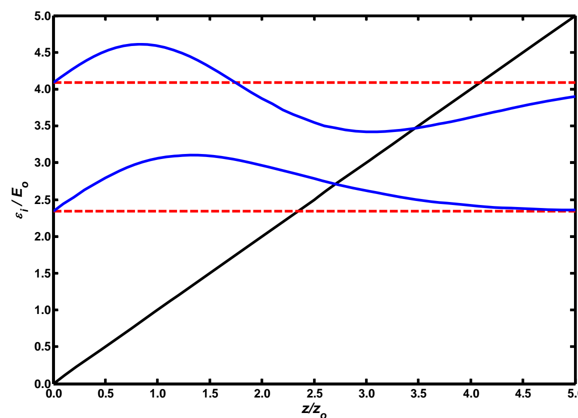

Fig. 2: Electron distribution in the first two quantized levels.

The saturation velocity obtained in Sec. III is utilized in modeling current-voltage (I-V) characteristics in Section IV. Sec. V gives an alternative description of the channel-length modulation that was a mistaken identity with inherent assumption of infinite saturation velocity that makes Ohm's law valid for all channel lengths. The concluding Section VI emphasizes the distinct features in modeling of the nano-MOSFET or any FET.

2. Quantum Confinement and Mobility

The channel in a nano-scale MOSFET is indeed a quantum-mechanical one that is constrained by the gate electric field forming an approximately linear quantum well (see Fig. 2). Contrary to the belief of many naïve researchers, no heating of the electrons by the gate is possible. Rather the gate confines an electron to length zQM comparable to the de Broglie wavelength. The energy spectrum is digital (quantum) in the z-direction perpendicular to the gate while other two Cartesian directions (x and y) are analog (or classical). This confinement makes the channel quasi two dimensional (QTD) [3-4]:

$$\varepsilon_{ki} = \frac{\hbar^2 k_x^2}{2m_1^*} + \frac{\hbar^2 k_y^2}{2m_2^*} + \varepsilon_i \tag{1}$$

with

$$\varepsilon_i = \xi_i E_o \approx \left[\frac{\hbar^2}{2m_3}\right]^{\frac{1}{3}} \left[\frac{3\pi q}{2} E_t \left(i + \frac{3}{4}\right)\right]^{\frac{2}{3}} \quad \text{i=0,1, 2, 3..} \tag{2}$$

$$E_o = \left(\frac{\hbar^2 q^2 E_t^2}{2m_3^*}\right)^{1/3} \tag{3}$$

where $k_{x,y}$ are the momentum vectors in the analog two-dimensional x-y plane and ε_i is the quantized energy in the digitized z-direction. $m_{1,2}^*$ is the effective mass in the x-y plane of the QTD channel and m_3^* is the effective mass in z-direction for a given conduction valley. ξ_i are the zeros of the Airy function ($Ai(-\xi_i)=0$) with ξ_0=2.33811, ξ_1=4.08795 and ξ_2=5.52056. As shown in Fig. 3, the conduction band energy surfaces are six ellipsoids with longitudinal direction along $\pm x,y,z$ in k-space [4] for <100>-oriented Si MOSFET . The two valleys have $m_3^* = m_\ell$ =0.98 m_o and four valleys have $m_3^* = m_t$ =0.19 m_o. $\varepsilon_o = \xi_0 E_o$ is the ground state energy corresponding to i=0 with m_3 = 0.916 m_o for the two valleys. Other four valleys are not occupied in the quantum limit when all electrons are in the lowest energy state. $m_{1,2}^*$ =0.19 m_o is the conductivity effective mass in the x-y plane of the QTD channel for lower two valleys. Electrons stay in the lowest quantized state appropriate for the two valleys that have a higher mass in the direction of confinement. In the x-y plane in which electrons are itinerant, the effective mass for these two valleys is the transverse effective

mass $m_t = 0.19\ m_o$ both for the density of states as well as for the mobility. E_t is the electric field generated by the gate, which in the strong inversion regime is given by [5-6]

$$E_t \approx \frac{V_{GT} + V_T}{6t_{ox}} \tag{4}$$

Here $V_{GT} = V_{GS} - V_T$ is the gate voltage above the threshold voltage V_T and t_{ox} is the thickness of the gate oxide.

Eigenfunctions corresponding to the eigenvalues in Eq. (1) are given by

$$\psi(x,y,z) = \frac{1}{\sqrt{L_x L_y}} e^{j\left(k_x x + k_y y\right)} Z_i\left(z\right) \tag{5a}$$

$$Z_i\left(z\right) = \frac{1}{Ai'\left(-\xi_i\right) z_o^{1/2}} Ai\left(\frac{z}{z_o} - \xi_i\right) \tag{5b}$$

$$z_o = \frac{E_o}{qE_t} \tag{5c}$$

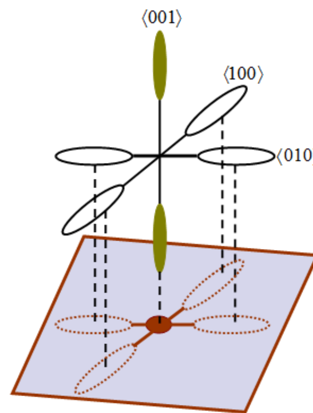

Fig. 3: The populated valley (filled) with quantum confinement in the z-direction with projection on the x-y plane with isotropic effective mass m_t=0.19 m_o.

The confined eigenfunctions $z_i(z)$ describing the standing waves in the approximate triangular quantum well ($V(z) = qE_t z$) at the gate and the corresponding eigenstates are shown in Fig. 2 for the first two digitized energy levels. The spacing between the two quantized levels may trigger the quantum emission when the energy gained $qE_\ell \ell_Q$ in an incoherent scattering length ℓ_Q on a tilted band diagram in the channel electric field is equal to $\hbar\omega_o = \Delta E_{1-0}$ multiplied by the probability $N_o + 1$ of emission with N_o the Bose-Einstein distribution. This gives incoherent scattering length

$$\ell_Q = \frac{E_Q}{qE_\ell} = \frac{(N_o + 1)\hbar\omega_o}{qE_\ell} \tag{6}$$

with

$$N_o = \frac{1}{e^{\hbar\omega_o / k_B T} - 1} \tag{7}$$

The average distance of the electron from the interface (z=0) for electrons in the ground state is [4]

$$z_{QM} = \frac{2}{3} z_o \tag{8}$$

The electrons do not reside at the Si/SiO_2 interface as wavefunction vanishes there due to the quantum-confinement effect shown in Fig. 2. The distance z_{QM} of the electrons that is a few nm cannot be neglected. In the nano-MOSFET the gate oxide is a few nm (t_{ox} = 1.59 nm in our case). Effective oxide thickness of the gate after correction for difference in permittivity of the SiO_2 and Si is given by

$$t_{oxeff} = t_{ox} + \frac{\varepsilon_{ox}}{\varepsilon_{Si}} z_{QM} \approx t_{ox} + \frac{1}{3} z_{QM} \tag{9}$$

The gate capacitance C_G is then lower than C_{ox} due to oxide thickness t_{ox} and is given by

$$C_G = \frac{\varepsilon_{ox}}{t_{oxeff}} = \frac{C_{ox}}{1 + \frac{1}{3}\frac{z_{QM}}{t_{ox}}} \tag{10}$$

Fig. 4 shows the effective oxide thickness with the increase in the gate voltage as electrons are squeezed closer to the interface. It is worth mentioning that there is another capacitance due to the depletion charge in the body of the MOSFET that is in series with the gate capacitance that does not affect the carrier concentration. This may affect the transient current in the body of the MOSFET, but in no way effects the dc characteristics being discussed here.

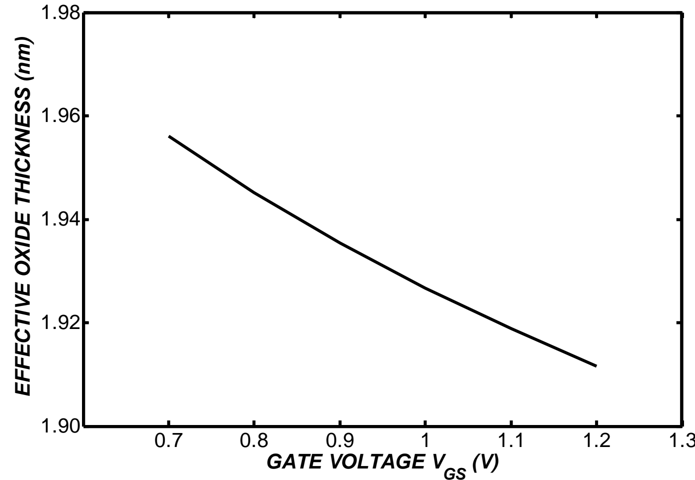

Fig. 4: Effective oxide thickness as a function of gate voltage with the quantum correction (t_{ox} = 1.59 nm).

Fairus and Arora [3] calculated the mobility for a QTD channel for isotropic scattering that includes the deformation potential acoustic phonon scattering, in fact any scattering that is proportional to the density of states. The mobility expression obtained is

$$\mu_{def} = \frac{2}{3}\frac{q\rho u_s^2 \hbar^3 L_1}{g_v m_t^2 E_{ac}^2 k_B T} \quad (11)$$

where ρ = 2330 kg/m^3 is the mass density, u_s = 8.43x10^3 m/s is the speed of sound, g_v=2 and E_{ac}=18.5 eV is the effective deformation potential constant, and T=300 K is the temperature. The effective width of the triangular-quantum-well channel is $L_1 = 2z_{QM}$. Lee, Spector, and Arora [8] have done extensive study of mobility affected by background and remote impurities in a quantum well. In a nanoscale channel, the two-dimensional electron gas is influenced by depleted back ground impurities in the depletion layer as well as by the remote positive sheet of the metal charge. The localized metal charge sheet may dramatically change the mobility due to decrease in the oxide thickness. The mobility due to the background ionized impurity scattering is given by

$$\mu_{imp} = \frac{32\hbar q k_B T}{N_I L_1 m_t}\left(\frac{\varepsilon}{4\pi Z q^2}\right)^2 \quad (12)$$

At room temperature and for N_I value presented in MOSFET, this mobility is much larger than the deformation potential scattering and hence does not contribute to the overall mobility. It is quite possible that the mobility in a quantum channel is barrier-limited and is controlled by processes distinctly different from a micro-channel. One such possibility is reflection of quantum waves from contacts which may yield an exponential behavior. No mechanism other than that given by Eq. (9) has been identified that may contribute substantially to the mobility. Rothwarf [3] has presented a quantum mechanical model of the channel mobility for Si MOSFET. His theoretical interpretation supports an empirical equation that summarizes experimental mobility for long channels to be given by

$$\mu = \frac{0.1105 m^2 / V.s}{1 + \left(\frac{E_t}{30.5 V / \mu m} \right)^{0.657}} \tag{13}$$

Fig. 5 gives the comparison of theoretical results from Eq. (9) to the experimental results summarized in the empirical Eq. (11). Considering that Eq. (11) applies to long channels, the agreement with experiments is very good. The possibility of ballistic mobility may transform this dependence. The mean free path calculated from Eq. (11) is in the range of 10-20 nm that is much smaller than 80 nm channel being considered here. Hence the effect of ballistic transport on mobility can be neglected.

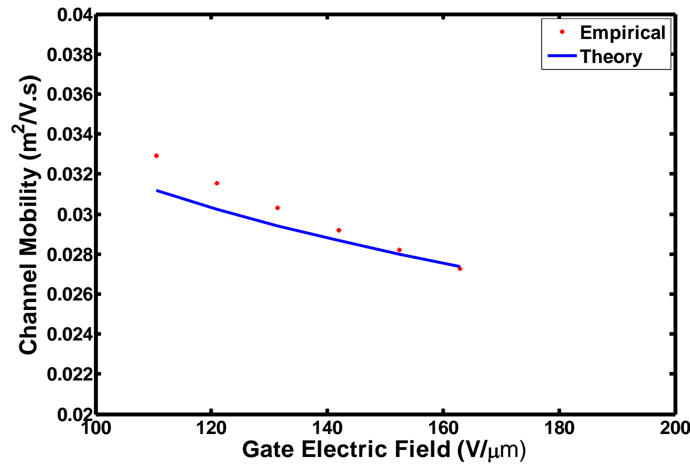

Fig. 5. The theoretical mobility calculated from the isotropic deformation potential scattering and compared with empirical results.

3. Transport in the Channel Electric Field

The carrier drift with electric field in the channel driving the electron has been explored in a number of works. Monte Carlo simulations, energy-balance theories, green functions, path integrals, etc. have been extensively tried. However, the fundamental issues relating velocity saturation and its relation to carrier mobility and scattering interaction continues to elude those doing modeling and simulations. A number of parameters is being tried in compact modeling of the data and are increasing as technology is entering the quantum and nanoscale domain. In the work of Arora [1], the ballistic transport, although not specifically mentioned by that name, was predicted in the presence of a high electric field. The theory developed was for nondegenerate bulk semiconductors that gave saturation velocity comparable to the thermal velocity. Recently, the theory has been extended to embrace all dimensions under both degenerate and nondegenerate conditions [10]. The ballistic nature of the velocity is apparent from Fig. 6 that streamlines the randomly oriented velocity vectors in a very high electric field. In the absence of external stimulation, the carriers are randomly oriented; their dipole energy $\pm qE_\ell \ell_o$ in a mean free path ℓ_o is also zero. However, as electric field is applied, the electron energy decreases by $qE_\ell \ell_o$ for electrons drifting opposite to the electric field and increases for those drifting parallel to the electric field. This creates two quasi Fermi levels (electrochemical potential) $E_F \pm qE_\ell \ell_o$ within one mean free path on each side of the location of a drifting electron (or a

hole). E_F is the Fermi energy related to carrier concentration. As conduction and valence bands and associated Fermi and intrinsic levels tilt in an electric field, electrons in the antiparallel directions are favored over those in the parallel direction finding it difficult to surmount the potential barrier with the net result that all carriers are drifting with the ballistic velocity in an infinite electric field. From traveling quantum wave perspective, the waves are reflected by the apparently insurmountable barrier in an intense driving field. The limiting intrinsic velocity for three-dimensional (bulk) nondegenrate electrons is shown to be $2\sqrt{2k_BT}\big/\sqrt{\pi m^*}$. The ballistic velocity reported by Lundstrom and Guo [11] is half of this value for the reason that the authors are considering only the average over one-half of the Maxwellian distribution. The drifting electrons are in a relay race, passing on their drift velocity to next electron at each collision, the velocity being unaffected by the collision. This is in direct contrast to the work of those researchers who believe in enhanced scattering for velocity to saturate. Published literature is inconclusive in predicting the dependence of high-field saturation velocity to low-field mobility. Often, the higher saturation velocity is indicated to arise from higher low-field mobility. This confuses the issue as to what scattering controls the mobility and what controls the saturation velocity. Arora's framework [1] includes all complicated scattering interactions into a single effective mean free path ℓ_o scalable under the strength of carrier scattering that leaves the saturation velocity unaltered and hence ballistic. The saturation velocity on the other hand is scaled by band structure parameters, unaffected either by the electric field or by the scattering that controls low-field mobility. Another difference between the work of [11] and that of [1] is that the ballistic velocity $\sqrt{2k_BT}\big/\sqrt{\pi m^*}$ quoted in [11] actually applies to bulk case not to the QTD gas being considered here.

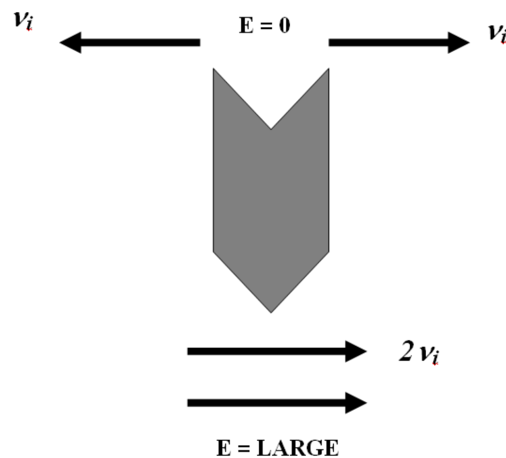

Fig. 6: Random motion in zero-field transforms to a streamlined one as extremely high electric fields are encountered.

The saturation velocity is the weighted average of the magnitude of the carrier velocity $|v|$ with weight equal to the probability given by the Fermi-Dirac distribution multiplied by the 2-dimensional density of states. This results in intrinsic velocity v_{i2} for a two-dimensional distribution given by:

$$v_{i2} = v_{th2} \frac{\Im_{1/2}(\eta_{F2})}{\Im_o(\eta_{F2})} \tag{14}$$

with

$$v_{th2} = v_{th} \frac{\Gamma(3/2)}{\Gamma(1)} = \frac{\sqrt{\pi}}{2} v_{th} = \sqrt{\frac{\pi k_B T}{2m_t^*}} \tag{15}$$

$$v_{th} = \sqrt{\frac{2k_B T}{m_t *}} \tag{16}$$

$$\Im_j(\eta) = \frac{1}{\Gamma(j+1)} \int_0^\infty \frac{x^j dx}{1+e^{x-\eta}} \tag{17}$$

$$\eta_{F2} = \frac{E_{F2} - E_{c2}}{k_B T} \tag{18}$$

Here E_{F2} is the Ferrmi energy of QTD carriers and $E_{c2} = E_{c0} + \varepsilon_o$ is the conduction band energy with the bandedge lifted by the quantum zero point energy of Eq. (2). The expressions obtained are in the quantum limit with only i=0 level being occupied for two valleys with lonitudinal axis in the direction of confinement ($m_3^* = m_\ell = 0.19m_o$). Other four valleys have the zero-point energy higher as the effective mass in the direction of confinement is $m_3^* = m_t = 0.916m_o$. Hence, ballistic velocity is appropriate for transverse effective mass $m_t^* = 0.19\, m_o$ for channel electric field in <100> direction. The Fermi energy however depends on the density-of-states effective mass m_d^* that for the lower two valleys is given by

$$n_s = N_{c2}\Im_o\left(\eta_{F2}\right) = N_{c2} \ln\left[1+\exp\left(\eta_{F2}\right)\right] \tag{19}$$

with $$N_{c2} = \frac{g m_d^* k_B T}{\pi \hbar^2} \tag{20}$$

With the electric field applied in the x- or y-direction for <100> oriented silicon, g =2 and $m_d^* = \sqrt{m_1^* m_2^*} = m_t^*$. The ballistic velocity in the nondegenerate regime is $v_{i2} = 1.96 \times 10^5\ m/s$. In the strongly degenerate regime, the ballistic (intrinsic velocity) is the Fermi velocity given by

$$v_{i2Deg} = \frac{2}{3} v_{F2} \tag{21}$$

$$v_{F2} = \sqrt{\frac{2\left(E_{F2} - E_{c2}\right)}{m_t^*}} = \sqrt{\frac{2\left(n_s \pi \hbar^2 / m_t^*\right)}{m_t^*}} = \frac{\hbar}{m_t^*}\sqrt{2\pi n_s} \tag{22}$$

4. Velocity Characteristics of Nano-MOSFET

The carrier density in the inverted MOSFET channel is normally degenerate. In this limit the drain velocity is given by Eq. (21) with n_s given by

$$n_s = C_G(V_{GT} - V_{Dsat}) / q \tag{23}$$

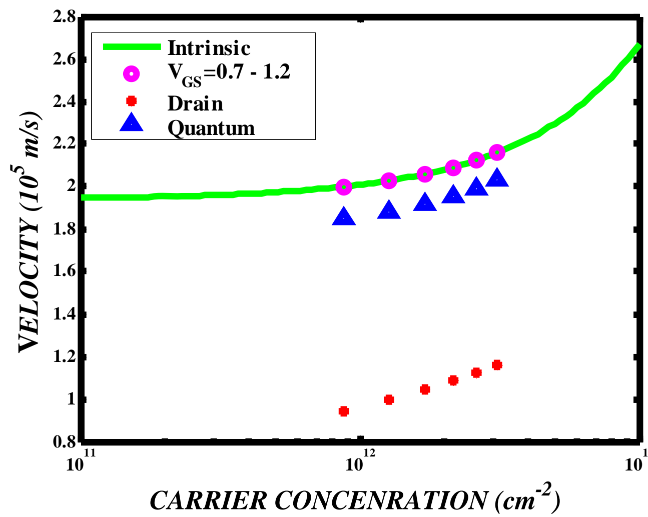

Fig. 7: The ultimate saturation velocity as a function of gate voltage. The saturation velocity increases as carrier concentration increases with the gate voltage.

The drain velocity is always smaller than that expected from an infinite electric field at the drain ($V_{Dsat} = V_{Dsat1}$ given below for $\alpha = 1$). The ultimate carrier concentration appropriate for the infinite electric field at the drain end (α=1) is obtained from Eq. (23) by replacement of V_{Dsat} with V_{Dsat1}. V_{Dsat1} itself depends on v_{sat} requiring an iterative solution with the nondegenerate saturation velocity $vsat = v_{th2} = 1.94x10^5$ *m/s* as the seed value. The calculated v_{sat} as a function of gate voltage is shown in Fig. 7. The solid line is the intrinsic velocity (the ultimate saturation velocity for an infinite electric field) obtained from Eq. (14) in the absence of quantum emission for T=300 K. The intrinsic velocity is independent of carrier concentration for low values and rises as a square root for high concentration. When calculated other temperatures (not shown), the intrinsic velocity in the degenerate domain is independent of temperature as given by Eq. (21). This is a significant shift from earlier works. The quantum emission lowers the saturation velocity as shown by triangles (▲). However the drain velocity (open circles ○) with which carriers leave the drain is lower due to the presence of a finite electric field.

The electric field at the drain E_D is given in Fig. 8. The assumption of carriers traveling with the ultimate saturation velocity is consistent with the infinite electric field at the drain (α=1) as shown by dashed lines which rise to infinite at the drain end. Under this assumption, the electric field is given by [13-15]

$$E_\ell = \frac{V_{Dsat1}}{2L}\frac{1}{\sqrt{1-\frac{x}{L}}} \tag{24}$$

The origin of V_{Dsat1} (see below) at the onset of current saturation is normally ascribed to the velocity reaching saturation at the drain end that is only possible if the electric field is infinitely large. The drain velocity $v_D = \alpha v_{sat}$ is a fraction α of the saturation velocity. The finite electric field at the drain gives for α an expression

$$\alpha = \frac{E_D / E_c}{1 + E_D / E_c} \tag{25}$$

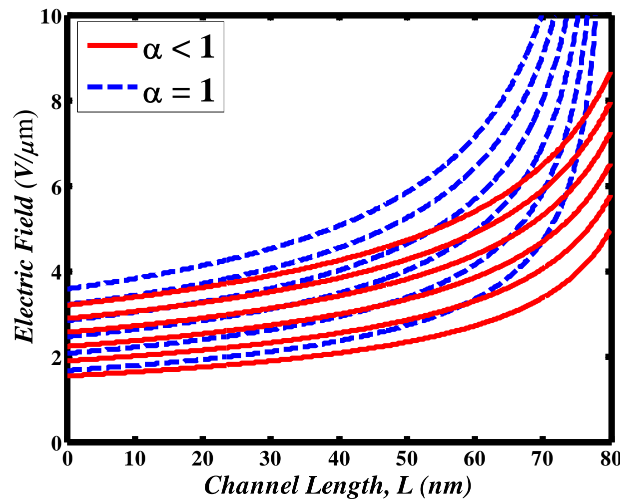

Fig. 8. Electric field profile (solid) with partial saturation ($\alpha \le 1$) and that (dotted) with full saturation ($\alpha = 1$).

The critical electric field for the onset of velocity saturation is $E_c = v_{sat} / \mu_o$. Since carriers leave the drain at velocity v_D, replacement of v_{sat} with $v_D = \alpha v_{sat}$ requires an iterative solution. The electric field profile with this iterative solution is indicated by solid lines in Fig. (8). As expected, the electric field is finite at the drain end (x=80 nm). The drain-to-saturation-velocity ratio α = v_D / v_{sat} is plotted in Fig. 9 as a function of drain voltage V_D starting from the saturation point V_{Dsat} to $V_D = 1.0\ V$. α and hence the associated drain velocity rises from its value at quasi-saturation current approaching 1 as the electric field increases due to increase in the drain voltage beyond saturation. α is higher for lower V_{GS} values. This is due to the fact that short channel effect arise when V_{GS} is larger than the critical voltage V_c=E_cL. V_{GS} being smaller is equivalent to channel length being larger as the ratio V_{GS}/V_c appears in the expression for I_{Dsat} and V_{Dsat} as shown below. Therefore, for long-

channel transistors, the value of α is almost closer to 1. This feature is clearly visible in long-channel I-V characteristics.

In the theoretical framework developed and described elsewhere [3, 9], the velocity-field characteristics in the presence of a driving electric field E of an arbitrary magnitude are given by

$$v = v_{sat} \tanh\left(\frac{E}{E_c}\right) = v_{sat} \tanh\left(\frac{V}{V_c}\right) \tag{26}$$

with

$$V_c = \frac{v_{sat}}{\mu_{\ell f}} L \tag{27}$$

$E=V/L$ when voltage V is applied across the channel. $\mu_{\ell f}$ is the low-field mobility that is lower than the bulk mobility because of change in the density of states by including the quantum confinement effects as stated in Sec. II. The velocity-field characteristics of Eq. (26) are plotted in Fig. 10.

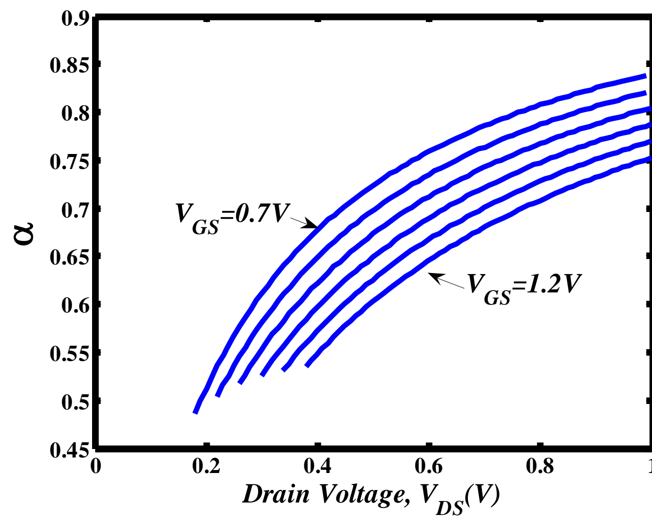

Fig. 9: The ratio $\alpha = v_D / v_{sat}$ of the drain velocity as a function of drain voltage beyond the onset of saturation $V_D > V_{DSAT}$ for V_{GS} =0.7 (topmost curve), 0.8, 0.9, 1.0, 1.1, and 1.2 (bottom curve).

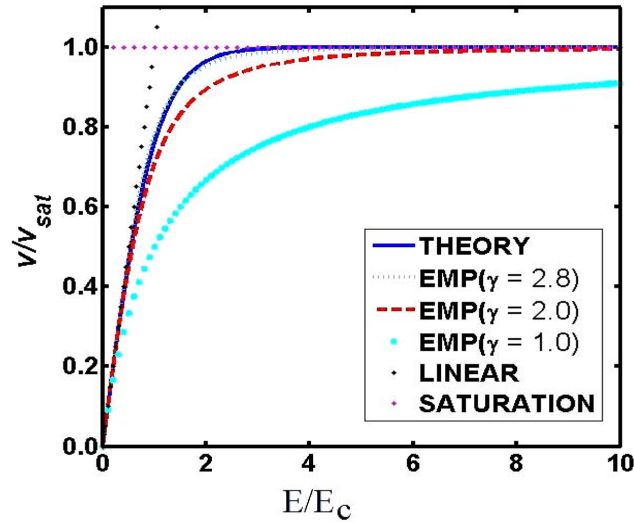

Fig. 10: Relative drift velocity versus relative voltage across a resistor from the theory of Eq. (19) and empirical models with as a parameter. Also shown are the saturation and ohmic lines.

The direct experimental test of Eq. (26) comes from the work of Greenberg and del Alamo [12] who have measured velocity in a 5-μm channel of InGaAs and shown that their results fit the empirical relation normally used in simulations. Their experimental data on a 5-μm InGaAs channel fits very well the empirical equation:

$$v = v_{sat} \frac{E/E_c}{\left[1+\left(E/E_c\right)^{\gamma}\right]^{1/\gamma}} \tag{28}$$

with γ = 2.8. A wide variety of γ values are cited in modeling and simulations. It is believed that $1 \le \gamma \le 2$ depending on the carriers (electrons or holes). Ref. 11 conclusively demonstrates γ = 2.8 for an InGaAs channel that is larger than 2. One reason for this apparent discrepancy arises from the fact that the highest velocity measured in a practically attainable high electric field is ascribed to be the saturation velocity. The infinitely large electric fields are impossible to attain in any functional device. The device will break down by a variety of mechanisms long before that high limit is reached. Therefore, it is impossible for carriers to attain the full saturation velocity (α=1). Fig. 10 compares the relative velocity of Eq. (26) with the empirical relation of Eq. (28) for γ =1, 2, and 2.8. The value of γ neither influences the linear domain nor the saturation domain. However, large value of γ makes approach towards saturation faster. γ=1 is convenient for transistor modeling and has been extensively used [12]. Since most carriers travel close to the saturation velocity in a nanoscale channel, the error introduced in using γ=1 is small and avoids another cycle of numerical integration by iterative analysis.

5. Current – Voltage Characteristics

The current-voltage characteristics for a MOSFET are obtained as [12]

$$I_D = \frac{C_G \mu_{\ell f} W}{L} \frac{\left(V_{GT} - \frac{1}{2} V_D\right) V_D}{1 + \frac{V_D}{V_c}} \qquad 0 \le V_D \le V_{Dsat} \tag{29}$$

Here V_D is the drain voltage with respect to source and V_{Dsat} is the drain voltage at which the drain velocity is maximum consistent with what is obtained from Eq. (14). The drain current at the onset of current saturation is given by

$$I_{Dsat} = \alpha C_G \left(V_{GT} - V_{Dsat}\right) W v_{sat} \tag{30}$$

Eqs. (29) and (30) must reconcile at $V_D = V_{Dsat.}$. This reconciliation [14] gives for V_{Dsat} and I_{Dsat} the expressions

$$V_{Dsat} = \frac{1}{(2\alpha - 1)} \left[(s - \alpha) V_c - (1 - \alpha) V_{GT} \right] \tag{31}$$

$$I_{Dsat} = \frac{\alpha}{(2\alpha - 1)} \frac{C_G \mu_{\ell f} W}{L} V_c \left[\alpha V_{GT} - (s - \alpha) V_c \right] \tag{32}$$

with $$s = \sqrt{\left[\alpha + (1 - \alpha)\frac{V_{GT}}{V_c}\right]^2 + 2\alpha(2\alpha - 1)\frac{V_{GT}}{V_c}} \tag{33}$$

The small-signal channel conductance g_{ch} and transconductance g_m are now obtained as

$$g_{ch} = \left.\frac{\partial I_D}{\partial V_{DS}}\right|_{VGT=const} = \frac{1}{2} \frac{C_G \mu_{\ell f} W}{L} \frac{2\left(V_{GT} - V_D\right) - \frac{V_D^2}{V_c}}{\left(1 + \frac{V_D}{V_c}\right)^2} \tag{34}$$

$$g_m = \left.\frac{\partial I_D}{\partial V_{GT}}\right|_{V_{DS}=const} = g_{mo} \frac{\frac{V_D}{V_c}}{1 + \frac{V_D}{V_c}} \;,\; g_{mo} = C_G W v_{sat} \tag{35}$$

The transconductance as a function of gate voltage is given in Fig. 11. Due to the lower drain velocity in $\alpha<1$ model the transconductance tends to be lower than predicted from full velocity saturation ($\alpha = 1$) model. g_m is below its limiting value g_{mo}. The transconductance in the saturation regime g_{m1} is

$$g_{m1} = g_{mo}\left[1-\frac{1}{\left\{1+\left(\frac{2V_{GT}}{V_c}\right)\right\}^{1/2}}\right] \tag{36}$$

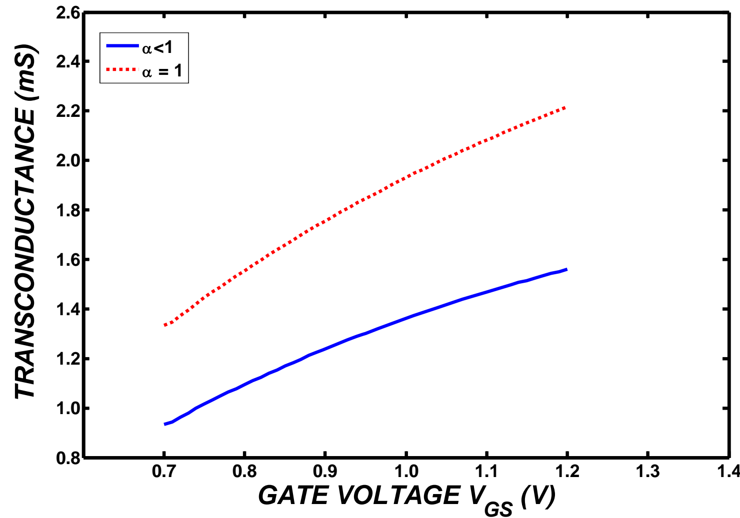

Fig. 11: The channel transconductance as a function of gate voltage for channel current at full saturation with α = 1 (dashed line) and partial saturation α = 1 < 1 (solid curve).

The channel conductance in the linear (triode) region is shown in Fig. 12. With α<1, no carrier has reached the ultimate intrinsic velocity at the saturation point giving $g_{ch} \neq 0$. In a model where α=1 the carriers are traveling at saturation velocity with an intrinsic assumption that the drain electric field is infinite. The channel conductance $g_{ch1}=0$ where dashed curve terminate in V_{Dsat1} in Fig. 12. However, when α<1, the solid curves of Fig. 12 terminate with a finite value of g_{ch} at $V_D=V_{Dsat}$. As explained earlier, for long channels (α=1), the drain velocity is closer to the ultimate saturation. However, for short channels α is always less than 1. Fig. 13 indicates the saturation current as a function of gate voltage. As is expected, there is a very little change in the saturation current in going from V_{Dsat} to V_{Dsat1} . When $\alpha=1$, Eqs. (31) and (32) simplify considerably and are given by

$$V_{Dsat1} = V_c\left[\sqrt{1+\frac{2V_{GT}}{V_c}}-1\right] \tag{37}$$

$$I_{Dsat1} = \frac{1}{2}\frac{C_G\mu_{\ell f}W}{L}V_{Dsat}^2 \tag{38}$$

Fig. 14 summarizes all the features stated so far and gives the I-V characteristics of an n-type nano-MOSFET of L=80 nm operating at room temperature. Solid lines are terminate at (V_{dsat} , I_{dsat}) coordinates for gate voltages V_{GS} = *0.7, 0.8, 0.9, 1.0, 1.1, and 1.2*. The dashed lines originating from (V_{dsat1} , I_{dsat1}) are appropriate to α=1 that gives zero

output conductance because of the flat slopes. The experimental results follow the α<1 slopes and put confidence in our theory as outlined above. The agreement is as good as can be given and no artificial parameters have been used in obtaining these curves. All equations utilized are physics-based. Fig. 14 also shows the envelope curves for the drain current passing through the saturation points in α<1 and α=1 models.

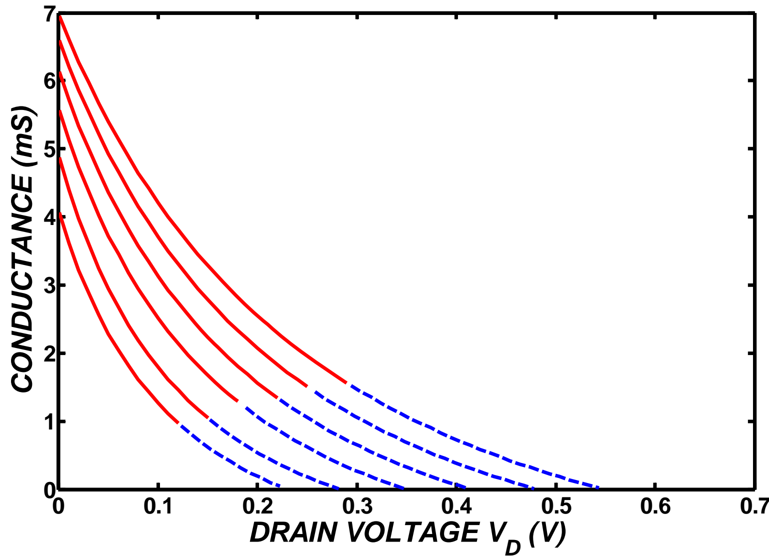

Fig. 12: The channel conductance as a function of drain voltage $0 \le V_D \le V_{Dsat}$ for V_{GS} =0.7, 0.8, 0.9, 1.0, 1.1, and 1.2. The conductance is finite at the onset of saturation (solid line). The dash lines cover the region $V_{Dsat} \ge V_D \ge V_{Dsat1}$.

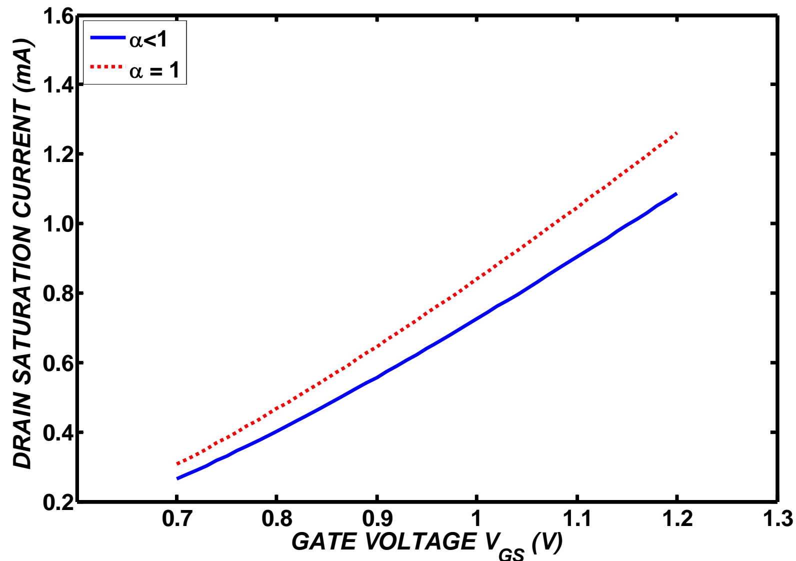

Fig. 13: The drain saturation voltage for channel current at full saturation with α = 1 (dashed line) and partial saturation α < 1 (solid curve).

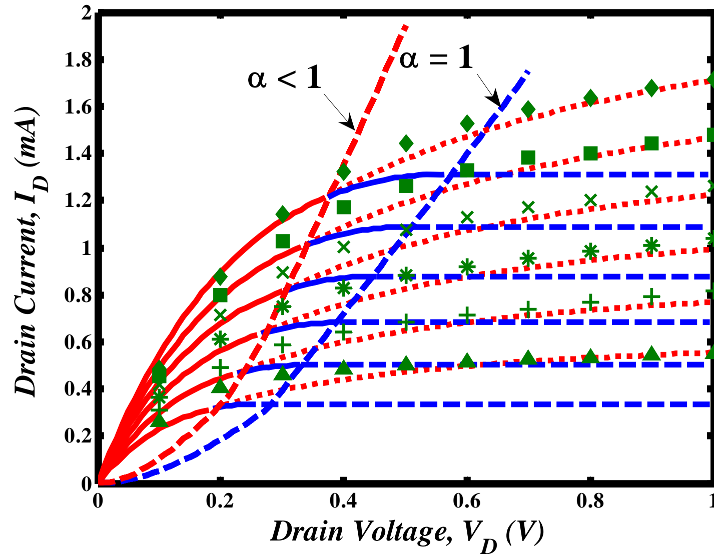

Fig. 14: I-V characteristics of 80-nm MOSFET for gate voltage V_{GS} =0.7, 0.8, 0.9, 1.0, 1.1, and 1.2. Solid lines are from Eq. (23) in the range $0 \leq V_D \leq V_{Dsat}$. The dotted lines are from Eq. (30) and are extension for $V_D \geq V_{Dsat}$. The dashed lines are for α =1.

6. Conclusion

The concentration-dependent saturation velocity replicates well the observed behavior in a nano-channel without using any fitting parameters. The pseudo channel length modulation in the absence of quasi-pinchoff and finite output conductance in I-V characteristics at the onset of drain saturation are well explained by velocity-field model based on the archival work of Arora [2]. In many ways, the distribution function reported [2] is similar to what is presented by Buttiker [16]. A series of ballistic channels of length ℓ comprise a macro-channel of length L. The behavior is well understandable as we consider ballistic low-field mobility where ℓ is replaced by L [17-19]. However, it does not affect the velocity saturation in high electric field that is always ballistic. The ends of each mean free path thus can be considered Buttiker's thermalizing virtual probes, which can be used to describe transport in any regime. In a high electric field, the electrons are in a coordinated relay race, each electron passing its velocity to the next electron at each virtual probe. The saturation velocity is thus always ballistic whether or not device length is smaller or larger than the mean free path. The ballistic saturation velocity is independent of the scattering-limited low-field mobility that may be degraded by the gate electric field. The relation between mobility and the mean free path has deep consequences on the understanding of the transport in any nanoscale device.

Natori [21] raised an inherent possibility of ballistic saturation velocity in his work. Our results are consistent with Natori's mindset. The fundamental difference lies in how saturation velocity is calculated. Similar to Buttiker probes mentioned above, Natori considers the net exchange of electrons that are injected into the channel from source and drain. The major difference arises from unidirectional nature of saturation velocity in a high electric field as considered here and only half the injected electrons going into the channel from either source or drain taken to be a reservoir of electrons. Good agreement with the experiment without the use of any artificial parameters is indicative of the fact that we have extended the vision of Natori to streamline electrons in a high electric field initiated by the electric field.

Considering these significant changes in modeling paradigm, we are confident that the results will benefit not only those doing modeling and simulations but also those who are doing fundamental physics.

Acknowledgement

The authors would like to thank Malaysian Ministry of Science, Technology and Industry (MOSTI) for a research grant for support of postgraduate students. The work is partially supported by the Distinguished Visiting Professor Grant # 77506 managed by the UTM Research Management Center (RMC). VKA thanks the Organizing Committee of the INEC2008 for their invitation. The excellent hospitality accorded to VKA by the Universiti Teknologi Malaysia, where this work was completed, is gratefully acknowledged.

References

[1] V. K. Arora, M. L. P. Tan, I. Saad, R. Ismail, Appl. Phys. Lett. **91** (2007)103510
[2] V. K. Arora, Jap. J. Appl. Phys. **24** (1985) 537
[3] A. Rothwarf, IEEE Electron Device Lett. EDL-8 **10** (1987) 499
[4] V. K. Arora, Microelectronics Journal **31** (2000) 853
[5] A. M. T. Fairus, V. K. Arora, Microelectronics Journal **32** (2000) 679
[6] F. Stern, Physical Review B **5** (1972) 4891
[7] M. L. P. Tan, R. Ismail, *J. Elektrika* **9** (2007) 37
[8] M. L. P. Tan, R. Ismail, R. Muniandy, W. V. Kin, Proceedings of the IEEE National Symposium on Microelectronics (2005) 210
[9] J. F. Cooper, D. F. Nelson J. Appl. Phys. **54** 3 (1983) 1445
[10] J. Lee, H. N. Spector, V. K. Arora, Impurity-Limited Mobility in a Quantum-Well Heterojunction **54** (1983) 6995: Quantum Transport in a Single Layered Structure for Impurity Scattering **42** (1983) 363
[11] V. K. Arora, Proceedings of the IEEE International Conference on Microelectronics, (2006) 17
[12] M. Lundstrom, J. Guo, *Nanoscale Transistor,* Springer, New York (2006)
[13] D. R. Greenberg, J. A. del Alamo, IEEE Transactions on Electron Devices **41** 8 (1994) 1334
[14] V. K. Arora, M. B. Das, Semiconductor Science and Technology, **5** (1990) 967
[15] J-W Chen, M. Thurairaj, M. B. Das, IEEE Transactions on Electron Devices **41** (1994) 465
[16] V. K. Arora, M. B. Das, Electronics Letters **25** (1989) 820
[17] M. Buttiker, Role of Quantum Coherence in Series Resistors Phys. Rev. B, **33** (1986) 3020
[18] J. Lusakowski, W. Knap, Y. Meziani, J. P. Cesso, A. El Fatimy, R. Tauk, N. Dyakonova, F. Boeuf, T. Skotnicki, Appl. Phys. Lett. **87** (2005) 053507
[19] M. Shur, IEEE Electron Device Letters **23** (1999) 511
[20] J. Wang, M. Lundstrom, IEEE Transactions on Electron Devices **50** (1999) 1604
[21] K. Natori, J. Appl. Phys. **76** (2000) 4879